WILEY-VCH

SUPPORTING INFORMATION

Effective Modulation of CNS Inhibitory Microenvironment using Bio-inspired Hybrid Nanoscaffold-based Therapeutic Interventions

Letao Yang, Brian Conley, Susana R. Cerqueira, Thanapat Pongkulapa, Shenqiang Wang, Jae K. Lee, and Ki-Bum Lee**

TABLE OF CONTENTS FOR SUPPORTING INFORMATION

A. METHODS:

Synthesis and characterization of MnO_2 nanosheets: To synthesize the precursor of MnO_2 nanosheets, we used a redox reaction between $MnCl_2$ and H_2O_2 following previous reports. Briefly, 2.0 mL of concentrated H_2O_2 (30 wt%) was added into an 18 mL solution containing 1.65 g Tetramethylammonium hydroxide pentahydrate ($TMAOH{\cdot}5H_2O$). After 10 minutes, under fast stirring at 1200 rpm using a magnetic stir plate, the second solution of $MnCl_2$ (0.375 g dissolved in 20 mL ultra-pure water) was quickly injected into the H_2O_2 and TMAOH solution. After continuing fast stirring for another hour, the stirring was slowed down to 400 rpm for another six hours to allow the reaction to complete. The MnO_2 precursor was harvested by centrifugation at 2000 round per minute (rpm) followed by water and ethanol washing three times each, and then the precipitates were dried in an oven at 60 Celsius overnight. Afterward, 100 mg precursor was crushed in 20 mL ultra-pure water and sonicated using a Brandson tip sonicator for three hours. The as-obtained MnO_2 nanosheet solution was further purified by centrifugation at 5000 rpm for 30 minutes and removal of aggregates. The concentration (mg/mL) of MnO_2 nanosheet in the solution was measured by evaporating 1.0 mL of the solution in a glass vial and measure the mass difference between the empty vial and the vial with dried MnO_2 nanosheets.

To characterize the MnO_2 nanosheets, transmission electron microscopy (TEM), Zeta sizer and Zeta Potential were used. In TEM imaging, a Philips CM12 TEM with 80 kilovolts voltage and an AMT digital camera model (XR111) were used. For the sample preparation, a diluted solution at 50 µg/ml was cast onto an EMS holey carbon TEM grids. A more concentrated solution at 500 µg/ml was used for the Zeta sizer and Zeta potential measurement.

Synthesis of 3D-BPH nanoscaffold: We adapted an LBL 3D electrostatic assembly strategy to synthesize the 3D-BPH nanoscaffold. Briefly, a highly viscous cationic polymer (e.g., chitosan solution at 2 wt%) was prepared and homogenized. Then a 20 µl droplet of the viscous solution was carefully transferred to the bottom of reaction vessels at designated shapes (e.g., cylindrical, tubular, pyramidal shapes). The 3D-assembly is initiated by the addition of 200 µl anionic MnO_2 nanosheet solution followed by incubation with the cationic polymer droplet. Due to the high surface tension, the cationic polymer slowly diffuses out and then binds to anionic nanosheets electrostatically in a layer-by-layer manner. Twelve hours after the addition of the nanosheet solution, the 3D-assembly was completed, and a dark-colored gel was formed. By freezing the gel at -80 Celsius followed by lyophilizing, a solid 3D-porous scaffold was obtained. To characterize the porous structures of soft biomaterials, lyophilization was used to maintain the integrity of pores, followed by FE-SEM imaging (lyophilization works through the sublimation of ice crystals and been extensively used for characterizing porous structures of hydrogels and porous scaffolds). [1-4]

The porosity of the 3D-BPH nanoscaffold was readily modulated by varying the concentration of MnO_2 nanosheets from 1.2 mg/mL, 1.8 mg/mL, 2.4 mg/mL and 3.0 mg/mL. As a control, water only (0 mg/mL MnO_2) was also added to the chitosan droplets; however, the as-formed solid after lyophilization was found to dissolve after a few hours of incubation in physiological conditions (cell culture medium, PBS, and pure water).

To load drugs (e.g., rhodamine B, or methylprednisolone) into the 3D-BPH nanoscaffold, concentrated solutions [methanol, dimethyl sulfoxide (DMSO) or water] of drugs were first dissolved in the aqueous solution of MnO_2 nanosheets. Afterward, we adapted the same procedures to induce the 3D-assembly and fabrication of 3D-BPH nanoscaffold. Thus, high concentrations of drugs can be loaded through both chemical (with MnO_2 nanosheets) and physical (encapsulation during assembly) forces.

In stem cell assays performed on the 3D-BPH nanoscaffolds, we functionalized scaffolds with cell adherent ECM ligands to support the adherence, growth, and differentiation of stem cells by incubation of 3D-BPH nanoscaffolds in concentrated laminin (100 μg/mL in PBS) solution for a short period (30-60 minutes) prior to the cell seeding.

Characterization of 3D-BPH nanoscaffold: The 3D-porous hybrid structures of 3D-BPH nanoscaffold were investigated by field-emission scanning electron microscopy (FE-SEM, Zeiss) with a gun voltage of 20keV. Samples were coated with 20 nm gold to enhance the conductivity. To analyze the pore structures in a more quantitative manner, mercury intrusion porosimetry (MIP, Micromertics Corp.) with a scanning range of 100 nm to 100 μm was used. Simulation on the porous structures was performed by COMSOL® software package. Briefly, SEM images were carefully outlined and refined in AutoCad to produce simulation geometry suitable for COMSOL software. A porous flow simulation was performed designating outlets, inlets, and boundaries for scaffold fluid flow. An assigned colormap indicates areas of high velocity and pressure. Smaller pore sizes exhibited lower velocity and higher pressure, while larger pores exhibited higher velocity and lower pressure. Overall, our simulation illustrates two key components of 3D-BPH nanoscaffold. First, there is ample interaction between the extracellular fluid environment and 3D-BPH nanoscaffold. This is essential for scaffold drug release and exposure to endogenous reductants for scaffold biodegradation. Second, the porous structure allows for cellular penetration and integration throughout the scaffold with access to proper metabolites provided by scaffold-fluid interactions.

To characterize the porous structure under hydrated conditions, we have also used a fluorescent microscope for imaging 3D-BPH nanoscaffold (synthesized from 2.4 mg/mL MnO_2 nanosheets) labeled with a high molecular weight dextran-TexRed dye. The labeled nanoscaffold was vigorously washed to remove the free-floating molecules and then imaged under a fluorescent microscope (Nikon Ti Series microscope). The pore size

distribution of the scaffold was then analyzed by NIS Elements software). A similar average pore size (47 μm) was observed as the FE-SEM characterizations, which is summarized in FIGURE S5.

To study the degradability of the 3D-BPH nanoscaffolds, the scaffolds (n=3 experimental replicates) with varying porosity were placed into a PBS solution of ascorbic acid at a concentration of 10 μg/mL. The degradation was monitored by the gradual disappearance of black color with the dissolution of MnO_2. When the scaffold becomes colorless and transparent, we record the time as the complete degradation time. It is important to note that the concentration of ascorbate human plasma is around 10 μg/mL, so the results obtained reflect the trend of the degradation from different porous nanoscaffold instead of the definitive degradation time *in vivo*.[5] To this end, we also performed biodegradation assay under more biomimetic conditions by forming a 3D-tissue around the 3D-BPH nanoscaffold via the seeding of a high density of fibroblasts cells that commonly exist in the different organs as well as at the SCI sites. A 10% FBS media in DMEM without the addition of any exogenous reductants or enzymes were used for the culture and mimic of the natural cellular microenvironment. Similar to the ascorbic acid-based degradation assay, we monitored the degradation of the scaffolds on a daily base based on the gradual disappearance of black color from the scaffold. Photographs were taken by a Nikon camera and summarized.

As matching mechanical strength between scaffold and tissue can be an important factor to consider for *in vivo* applications, we also used AFM to characterize Young's modulus of the scaffolds (n=3-4 experimental replicates) with different porosities. By using a high-resolution AFM tip (from Park Systems), we used contact mode and generated the force value versus distance graphs for the scaffolds. From the graphs, we then calculated Young's modulus of the scaffolds. Also, to characterize the single pore structure of 3D-BPH nanoscaffold (synthesized from MnO_2 nanosheet concentration of 2.4 mg/mL with an expected pore size of 50 μm), we used a liquid cell set-up in the AFM measurement through non-contact mode. A low scanning frequency (0.2 Hz) was used to minimize noises during the measurement of 3D flexible structures in the nanoscaffold.

To create a favorable and biomimicry ECM for the growth and differentiation of neural cells, laminin and bFGF was coated to the 3D-BPH nanoscaffolds (average weight of 1.5 mg, n=4 experimental replicates) after one hour (FIGURE 3F) or 24-hour (FIGURE S7) incubation in a concentrated (100 μg/mL) laminin and a bFGF PBS solution, respectively. The amount of laminin absorption was quantified by BCA assay and based on the differences before and after the scaffold absorption. As controls, polymer- (polycaprolactone), 3D-chitosan (lyophilized from chitosan solutions) and glass-based scaffolds were also incubated with the same concentration of laminin solution and calculation of protein concentration using BCA assay. The protein concentration was reflected by the absorption of Copper (II) ions at 570 nm, which was recorded by a standard Tecan plate reader.

The loading of the drug is quantified using a similar approach. For the model fluorescent drug (rhodamine B), scaffolds were soaked in a 50 μg/mL PBS solution of rhodamine B for overnight, then the fluorescence intensities

of the supernatant before and after were recorded for the calculation of drug absorption. Rhodamine B (RhB) is a commonly used model drug for characterizing drug release from nanoscaffold, and the quantification during drug release based on rhodamine B is often more reliable due to the high absorbance of rhodamine B around the wavelength of 500 nm.[6] For the anti-inflammatory drug (MP), UV-Vis absorption spectroscopy was used to quantify the drug loading efficiency. MP drug concentration at 50 μg/mL was used for the loading as well as the subsequent anti-inflammatory studies. Due to the relatively low solubility of MP, we first prepared a concentrated solution (1.0 mg/mL) of MP in ethanol then the solution was diluted to reach the 50 μg/mL concentration for the drug loading. When the drug was loaded during the formation of the scaffolds, the percentage of loaded drugs is nearly 100%, as all drugs should be encapsulated inside the scaffold during the 3D-assembly.

In vitro drug-release assay: To investigate the drug release profiles from 3D-BPH nanoscaffolds at varying porosities, 100 μg rhodamine B was loaded into 1.0 mg scaffolds during the 3D-assembly. Afterward, the scaffolds were briefly washed in PBS before we started the quantification of the drug release amount. At different time points of Day 1, Day 2, Day 4, Day 7, and Day 14, we collected the supernatant and measured their absorption using the distinctive peak around 500 nm. As a control, we also studied the release profile of Rhodamine B from a polymer scaffold (PCL nanofiber) by mixing the same amount of rhodamine B into a PCL solution followed by an electrospinning process to form the nanofiber matrix. PCL is selected as a control as it is one of the mostly used nanoscaffold compositions for tissue engineering and treating spinal cord injury.[7-8] The supernatant from the rhodamine B-loaded PCL nanofiber was collected on the first day and compared to the 3D-BPH nanoscaffold. These drug release profiles were summarized in the graph in FIGURE 3.

In vitro anti-inflammation assay: For the *in vitro* studies on the inflammatory responses, we focused on human macrophages. More specifically, using the THP-1 monocyte cells derived from humans, we converted them into adherent macrophages via the treatment of 500 ng/mL PMA into the growth media of monocytes for 48 hours. To initiate the inflammatory response, 1.0 μg/mL LPS was added into the media of macrophages for 4 hours (unless specifically stated at different lengths of time) before the cells were washed with regular THP-1 culture media. The inflammatory responses were checked by gene analysis using qRT-PCR (n=3 experimental replicates) and the PMA-converted macrophage without LPS treatment was used as the control (n=3 experimental replicates) [TABLE S1-S2]. After the confirmation of macrophage activation by LPS, anti-inflammatory effects from MP-loaded 3D-BPH nanoscaffolds (MP-scaffold) were then investigated using a Transwell® platform. Briefly, monocyte was cultured in the bottom layer of Transwell® followed by PMA and LPS treatment. After changing the media into the normal growth media, the MP-scaffolds were placed on the top membrane of the Transwell®

and additional media was added until the scaffolds were covered. The cells were incubated with the MP-loaded scaffolds for 24 hours before their gene expression on the inflammatory markers (TNF, IL-8, IL-6, CXCL1, CCR7, and CCL5) and anti-inflammatory markers (IL-4, IL-13) from the macrophages were checked by qRT-PCR. Additionally, we have performed a study on the anti-inflammatory effect from the scaffold alone (without drug loading) based on the TNF gene expression in macrophages. Although there is a slight decrease in TNF expression in the 3D-BPH nanoscaffold (without drug loading), the difference is insignificant. The slight decrease of TNF expression induced by the scaffold incubation might originate from the ability of the scaffold to absorb inflammatory factors (e.g., LPS and TNF), and the insignificant difference suggests such effect do not play an important role in the current anti-inflammatory study.

In vitro stem cell differentiation assays: The ability of 3D-BPH nanoscaffolds to promote neurogenesis *in vitro* was examined by the neuronal differentiation of hiPSC-NSCs inside the 3D-BPH nanoscaffolds (n=3-5 experimental replicates). More specifically, hiPSC-NSCs were seeded into the laminin-coated 3D-BPH nanoscaffolds at a high density (1 million per well in a 48-well plate) and allowed to adhere, proliferate and integrate for 24 hours using the bFGF formulated media. Afterward, the media was switched into differentiation media with bFGF withdrawal. The media was changed every other day during the differentiation process. 7-day (for short-term neurogenesis studies) or 14-day (for long-term maturation studies) post the bFGF withdrawal, cells were washed by PBS and then fixed using formalin. The differentiation of hiPSC-NSCs into neurons has been studied in several reports, and it is generally known that there are majorly two stages of differentiation. In their early stage (typically within a week), early neuronal markers are expressed, and TuJ1 is the most representative marker. In the later stage (typically 1-4 weeks), mature neuronal markers such as microtubule-associated protein II (MAP2), Synapsin (SYN), and Hexaribonucleotide Binding Protein-3 (NeuN) will express. Therefore, to systematically study the early stage and late-stage neuronal differentiation of hiPSC-NSCs on the 3D-BPH nanoscaffolds, we investigated early neuronal marker (TuJ1, at Week 1) and mature neuronal markers (MAP2, SYN, and NeuN, at Week 2) in the differentiated neurons. As controls, laminin-coated glass substrate and chitosan scaffold were used to induce the differentiation of hiPSC-NSCs using identical procedures performed on the 3D-BPH nanoscaffolds.

In vitro neuroinflammation assay: After confirming the ability of 3D-BPH nanoscaffolds to provide a favorable 3D-biomimetic ECM for neurogenesis, we then sought to study the inspect the enhanced survival and neurogenesis under inflammatory conditions by co-delivering MP. To this end, a neuroinflammation co-culture model was first established. More specifically, in a Transwell® system, we seeded THP-1 cells at a high density,

converted them using PMA and activated the macrophages using LPS following the identical protocols mentioned above. Meanwhile, hiPSC-NSCs were seeded to the 3D-BPH nanoscaffolds or control scaffolds (glass and chitosan-based) (n=4-5 experimental replicates) using the same method in the neuronal differentiation assay. Afterward, the cell-seeded scaffolds were placed on top of the membrane of Transwell® and a co-culture media (5% FBS in hiPSC-NSC media) was added into the well. Macrophages were stimulated every other day for four hours, followed by immediate media change into the co-culture media. The differentiation was continued for 7 days before the cells were fixed and stained. To further examine the combined therapeutic effects with the delivery of MP, we repeated the same co-culture assay, and the MP-loaded 3D-BPH nanoscaffolds were used instead of the scaffolds alone. For the control glass scaffold, an initial addition of MP for absorption and loading was performed followed removal right before the cell assays. For the chitosan scaffold, the same amount (50 μg/mL) of MP was loaded using the identical approach (mixing MP with chitosan solution followed by lyophilization). By comparing the cell survival using nuclei count and neuronal differentiation by the percentage of TuJ1 positive cells, the effects from MP can be concluded by comparing the MP-loaded scaffolds and plain scaffolds alone. By comparing the cell survival and neuronal differentiation from the assay of MP-loaded 3D-BPH nanoscaffolds and the other two control scaffolds (glass, and 3D-chitosan scaffolds, FIGURE 4g-j), we can also further support the advantages of the 3D-BPH nanoscaffolds compared to the conventional scaffolds in promoting neurogenesis under inflammatory conditions.

Cell SEM imaging: After seven days of hiPSC-NPC neurodifferentiation, 3D-BPH nanoscaffolds were chemically dried by incubating with 25%, 50%, 75%, and 100% ethanol changing each solution every 30 minutes. Afterward, samples were lyophilized for 24 hours. Prior to SEM imaging, each sample was coated with approximately 20 nm of Au to improve conductivity. SEM images taken were representative of i) degree of porosity and ii) three-dimensional attachment of cells. To this end, it is clear that neurite outgrowth extended throughout the porous structure to initiate neural network formation in 3D-BPH nanoscaffolds.

In vitro immunostaining for protein analysis: Immunostaining was used for the study on the *in vitro* neurogenesis of hiPSC-NSCs on the 3D-BPH nanoscaffolds as well as control scaffolds. Previous protocols on the immunostaining were adapted to the current experiments. Briefly, after we fix cells using formalin, we permeabilize cells using blocking buffer (5% normal goat serum from Life Technologies and 0.3% Triton X-100 dissolved in PBS) for one hour at room temperature. Then the primary antibodies of TuJ1 (mouse, from Biolegend with the catalog number of 801202 and at a 1:500 dilution), MAP2 (mouse, from Cell Signaling with the catalog number of 8707S and a dilution factor of 1:500), Synapsin 1 (rabbit, from Sigma Aldrich Millipore with the

catalog number of AB1543P and a dilution factor of 1:300), NeuN (mouse, from Biolegend, with the catalog number of 834501 and a dilution factor of 1:400) dissolved in antibody dilution buffer (1% bovine serum albumin, 0.3%Triton X-100 in PBS) were added to the cells. After incubating for one hour at room temperature, cells were washed by PBS for three times (5 minutes each) and secondary antibodies dissolved in antibody dilution buffer were added and incubated for 1.5 hours at room temperature. Among them, an anti-mouse antibody labeled with Alexa 594 dye was purchased from Biolegend with the catalog number of 8890 at a dilution factor of 1:300. The anti-rabbit antibody labeled with Alexa 488 dye was also purchased from Biolegend with the catalog number of 406416 and a dilution factor of 1:300. With the completion of antibody staining, we also stained cell nuclei with DAPI (from Life Technologies, with the Catalog Number of D1306 at a 1:100 dilution and 30 minutes of incubation) to count cell numbers.

In vitro qRT-PCR for gene analysis: We analyzed the neuronal and inflammatory genes using qRT-PCR in our study (n=3 experimental replicates). Typically, we extracted the total RNA of neural cells and macrophages using TRIzol purchased from Life Technologies. Afterward, the mRNAs were converted into cDNA by using the Superscript III First-Strand Synthesis System from Life Technologies. Then a Power SYBR Green-based PCR Master Mix on a StepOneplus PCR system from Applied Biosystems was used to perform the qPCR reactions. Ct values for each gene of interest were normalized to GAPDH based on our previous protocols. In all reactions, we used the standard cycling conditions by setting a melting temperature of 60 °C . The primers for each gene of interest were designed based on the PrimerBank database and purchased from IDT. The sequences of each gene in the qRT-PCR experiment are summarized in TABLE S1. [9-11]

Fluorescent imaging and image analysis on the in vitro neuronal differentiation assay: Fluorescent imaging on the neuronal differentiation assay and neuroinflammation co-culture model was performed on a Nikon Ti Series microscope and Zeiss LSM 800 confocal microscope. As the 3D-BPH nanoscaffold is non-transparent, samples were inverted and facing toward the objectives during the imaging. For the image analysis, the number of total cells was quantified by ImageJ or Nikon NIS AR software based on the automatic identification of cell nuclei using the DAPI marker. The amounts of cells that are considered positive for each specific neuronal marker (TuJ1, MAP2, Synapsin, and NeuN) were also measured by manual counting due to its 3D imaging nature which makes it difficult to be analyzed by ImageJ. The percentage of marker-positive cells can be calculated from the number of marker-positive cells divided by the total cell numbers. Axonal lengths were evaluated by the NeuronJ package in the Image J software. Sample number “n” means the number of measurements from individual experiments (n=5 and 9 technical replicates in FIGURE 4, and FIGURE S9, respectively). Error bars are the

standard deviation of the mean unless stated otherwise, #P<0.1, *P<0.05, **P<0.1, ***P<0.001 by one-way ANOVA with Tukey post-hoc analysis.

In vivo scaffold transplantation assay: Female adult C57BL/6J mice (8-10 week-old; Jackson Labs, USA) were housed according to the National Institutes of Health (NIH) guidelines, and the Institutional Animal Care and Use Committee of the University of Miami approved all animal procedures (Animal Welfare Assurance Number A3224-01, protocol no. 17-121; PI Jae K. Lee). Mice were anesthetized [ketamine/xylazine, 100 mg/15 mg/kg intraperitoneal (i.p.)] and the back of the animal was shaved and aseptically prepared with chlorhexidine solution before surgery. A dorsal laminectomy was performed at thoracic vertebra T8, exposing the surface of the spinal cord. The dura was punctured using a 30G needle, and pair of superfine iridectomy scissors were used to cut the dorsal half of the spinal cord at a depth of 0.8mm. Animals were randomly assigned to experimental groups at the time of scaffold implantation, and surgeons were blinded to the treatment groups. Control (n=11 animals) or the MP-scaffold (~10 μg) (n=12 animals) were carefully inserted into the lesion. The muscles were then sutured, and the skin closed with clips. All injured mice received Lactated Ringer's solution, antibiotics (GentaMax100, 10 mg/kg), and analgesics (Buprenex, 0.05 mg/kg) subcutaneously for the first week after surgery. Twice daily bladder expressions were done for the entire duration of the study. The number of animals used in this study was calculated from a power analysis of the variance obtained in a pilot study to determine statistical power for the behavioral analysis (α=0.05; power=0.8).Locomotion recovery (n=12 and 11 animals for the experimental and control groups, respectively) was assessed using the Basso Mouse Scale at 1 day and weekly after injury. The hind limb movement was scored in an open field from 0 (no observable hindlimb movement) to 9 points (normal locomotor function) (Basso et al., 2006). Two examiners blinded to the treatment group performed all locomotor assessments. Animals were also scored 1-day post-SCI to confirm the lesion severity. Three mice (1 from control and 2 from MP-scaffold) that scored 3 or higher at this time point (plantar placement or stepping) were excluded from the study.

Additional discussion in the potential systemic cytotoxicity from 3D-BPH nanoscaffold: Although manganese is widely known as an essential element for human with a required daily uptake at 1.2-2.2 mg, previous literature has suggested the administration of a high dosage of manganese compounds can cause toxic effects. Therefore, we have carefully calculated the amount of MnO_2 nanomaterials transplanted into each mouse to ensure a proper dosage. Typically, 10 μg of the 3D-BPH nanoscaffold was transplanted into a mouse with average weights around 25g, corresponding to a maximum dosage of MnO_2 nanomaterials at 0.4 mg/kg, as the 10 μg of nanoscaffold include both chitosan and MnO_2 nanomaterials. The dosage of 0.4 mg/kg is extremely low compared to the

commonly reported toxic dosage for MnO_2 nanomaterials *in vivo* [(J Appl Toxicol. 2013 Oct; 33(10):1165-79. doi:10.1002/jat.2887).

In vivo qRT-PCR assay for inflammatory gene analysis: Inflammatory gene expression was evaluated in mice that received a dorsal hemisection SCI (as described above) with control (n=5 animals) or MP-scaffold (n=6 animals) implantation. At 24 h after SCI, mice were perfused transcardially with ice-cold Diethylpyrocarbonate (DEPC)-PBS. A 4-mm spinal cord segment centered at the injury site was dissected and homogenized. Total RNA was extracted from the injury site using TRIzol (ThermoFisher Scientific, USA) and purified using the Ambion PureLink RNA Mini Kit (ThermoFisher Scientific, USA), according to the manufacturer's protocol. cDNA was synthesized using iScript cDNA Synthesis Kit (BioRad, USA). Quantitative PCR was performed using QuantStudio 6 Flex Real-Time PCR System in a 384 well-plate format with Fast SYBR Green Master Mix (ThermoFisher, USA). Primers were designed to span introns and generated using Primer-BLAST (Table 1). Sample threshold cycle (CT) values for each gene were normalized to that of Gapdh and converted to ΔΔCT using the following equation: $\Delta\Delta CT = \log2(-(CTGene - CTGapdh))$.

In vivo immunostaining assay: Animals were transcardially perfused with ice-cold 4% paraformaldehyde (PFA, 0.1M PBS, pH 7.4) 28 days after SCI and scaffold implantation. The brains and spinal cord were removed, post-fixed for 2 h, and cryopreserved in 30% sucrose solution for 48h at 4 °C. An 8-mm segment of the spinal cord centered at the injury site was embedded in OCT compound (Tissue Tek, USA), and cut into serial sagittal sections (16μm thick). Sections were washed in PBS and then incubated in a blocking solution of 5% normal donkey serum with 0.3% Triton X-100, for 1 h at room temperature. Next, the tissue was immunostained for CD11b (Invitrogen, 1:500), GFAP (Abcam, 1:500), PDGFRβ (Abcam, 1:200) and 5-HT (ImmunoStar, 1:200) by incubation in primary antibody solution overnight at 4 °C. After washing in PBS, Alexa Fluor secondary antibodies were added to the sections for 1 h (Invitrogen, 1:500), and DAPI (Invitrogen, 1:10,000) for 5 minutes. Sections were cover-slipped with Immumount mounting medium (Thermo Scientific, USA) and maintained at 4 °C until imaged in an Olympus VS120 Virtual Slide microscope (Olympus, USA).

***In vivo quantification of spinal cord tissue slices*:** All tissue slices stained with CD11b, GFAP, PDGFRβ and 5-HT were blindly analyzed to determine their suitability for analysis (e.g., tissue damages and folding, as well as whether showing clear features of injuries). More specifically, tissue images with improper injury severity (excluding slices with injuries greater than 75% damaged tissues around the epicenter and less than 25% tissues showing injury features) were not included for the analysis due to poor qualities (FIGURE S12). Stitched

fluorescent images for the whole spinal cord tissues around the injury sites of both the control and experimental group were taken under identical experimental settings for consistency. For the analysis on the CD11b, GFAP, PDGFRβ markers (n=8 and 9 animals from the experimental and control group, respectively), we performed fluorescent imaging on 4-5 separate layers for one animal. Afterward, the images were automatically analyzed by a Nikon Elements AR software in terms of the macrophage infiltration area, glial scar area and fibrotic scarring intensities. More specifically, the Nikon Elements AR software has a module with logarithms for automatic detection of specific tissue regions based on fluorescent contrasts. The software will then automatically isolate the region of interest and output the area, fluorescent intensities and perimeters. The area values were used for quantifications of macrophage infiltration and astroglial scarring formation. The fluorescent intensity was used for the quantification of fibrotic scarring. All data points plotted in FIGURE 5g-i were for individual animals and were averaged from result of the 4-5 layers of the same animal. To analyze the axon growth after injuries, 5-HT immunofluorescent staining (n=7 animals for both control and experimental groups) were blindly, and semi-automatically, traced using NeuronJ (from ImageJ), solely focusing on the caudal region. In the summarized graph in FIGURE 6e, 4-5 sagittal tissue sections from each animal were analyzed and then averaged for the quantification. Specifically, axons were analyzed from the 2D sections of spinal cord tissue and the number of axons within 100 μm distance intervals (i.e. 0-100 μm, 100-200 μm, etc.) was quantified through the use of MATLAB.

Statistical analysis: All statistical analysis and plotting of graphs were performed by GRAPHPAD Prism® and Origin and illustrated by CorelDraw® software packages. For the comparison of two samples, the Student's t-test was used. For the comparison of more than two samples, one-way ANOVA with Tukey post-hoc analysis was used. Significance levels were determined at levels of *P<0.05, **P<0.01, ***P<0.001. Individual data points were plotted in the bar graphs with n=experimental number or animal number unless specified otherwise. Error bars are standard deviation (S.T.D.) around the mean except for FIGURE 6f, where error bar represents standard error around the mean.

Synthesis and degradation of GO-chitosan 3D scaffolds: GO-chitosan scaffold and chitosan scaffold were synthesized to support the degradability and enhanced neuronal differentiation, respectively. To generate the GO-chitosan scaffold, a 20 ul droplet of concentrated (3wt%) chitosan aqueous solution was placed onto the bottom of a test tube, followed by incubation with 1.0 mL concentrated GO solution (2.4 mg/mL, the same concentration as the 3D-BPH nanoscaffold with optimal performance in the neurogenesis assay). The GO was synthesized and processed based on our previous publications. 12 hours after the addition of the GO solution, the electrostatic-

based 3D assembly was completed, and a dark-colored gel was formed, similar to the 3D-BPH nanoscaffold. By freezing the gel at -80 Celsius followed by lyophilizing, we then obtain the control GO-chitosan 3D scaffolds.

We checked the degradation of GO-chitosan 3D scaffolds following the identical procedures reported for the 3D-BPH nanoscaffolds. Briefly, the dark-colored scaffolds were incubated with 10 μg/mL ascorbic acid in PBS or 1 million cells per well in a 48 well plate, and then the color of the scaffold was monitored throughout a 2-week process. Photographs were taken every other day. As expected, no noticeable disappearance of the black color was observed, thereby confirming the intrinsic degradability of 3D-BPH nanoscaffolds are from the chemical formulation (MnO_2-based 3D assembly) instead of the chitosan or the 3D porous structure. The control chitosan scaffolds were produced by placing a 20 μL droplet of concentrated chitosan in a test tube followed by incubation with ultrapure water for 12 hours before lyophilization. For the differentiation assays, the lyophilized powders were washed with water followed by coating with laminin using the same conditions as the 3D-BPH nanoscaffolds.

Synthesis of MnO_2-PEI 3D scaffolds: To study the effects of different cationic polymers on the properties of 3D-BPH nanoscaffolds, we also initiated 3D assembly between MnO2 nanosheets and polyethyleneimine polymer with medium-range (10-20k molecular weight) of sizes. More specifically, a 20 μl droplet of the viscous PEI solution (3 wt%, Sigma Aldrich) was placed on the bottom of a test tube and then incubated with 2.4 mg/mL MnO_2 nanosheets overnight before they were lyophilized. An optical microscope (Nikon Eclipse Ti series) was used to monitor the overall structure of the scaffold. To study the interactions between NSCs and the PEI-based 3D-BPH nanoscaffolds (3D-BPH-PEI nanoscaffold), we seeded fluorescently labeled NSCs to the 3D-BPH-PEI nanoscaffold. One day after the seeding, we imaged cell morphology under a fluorescent microscope and found unhealthy (spherical and shrunk) cell morphology, as well as a low cell density, compared to those cultured in 3D-BPH nanoscaffold, suggesting a potential toxic effect from PEI in the 3D scaffold.

Solvent effects on the synthesis of 3D-BPH nanoscaffolds: We examined the solvent effects on the 3D assembly by replacing the water into another polar solvent with a lower viscosity (dimethylformamide). Briefly, MnO_2 precursors were suspended into dimethyl formamide (DMF) followed by extensive tip sonication. Afterward, the solution was incubated with the chitosan droplet, froze at -80℃ and lyophilized as described for the 3D-BPH nanoscaffolds. We found the scaffolds were mostly in the form of condensed sheets. The non-porous and highly condensed structure was further imaged and confirmed under SEM.

Microfluidic drug elution assay: One of the advantages of scaffold-based drug delivery is the reduced side effects of local drug delivery. To confirm the spatially controlled drug delivery by 3D-BPH nanoscaffolds, we created a single-channel microfluidic platform with a channel diameter similar to a normal-sized blood vessel (1 mm) at a flow rate similar to common blood flow (~1.2 m/s). Briefly, to mimic the inflammation in a mouse spinal cord tissue, macrophage cells were seeded into a microfluidic channel with a diameter of 1.0 mm with a constant unidirectional media flow (from left to right) that represent the fluidic condition at the injury sites. Afterward, a vertical channel on the top of the existent channel was formed by a PDMS puncher, followed by the insertion of a model fluorescent drug (RhB)-loaded 3D-BPH nanoscaffold into the vertical channel. A model drug rhodamine B (RhB) was used for visualization purpose. RhB is loaded during the assembly using identical protocols described in the drug releasing Methods section. Besides, to load drugs into the 3D-BPH nanoscaffold, concentrated solutions of RhB were first dissolved in the aqueous solution of MnO_2 nanosheets. Afterward, we adapted the same procedures to induce the 3D-assembly and fabrication of 3D-BPH nanoscaffold. By monitoring the diffusion of the fluorescent drug, we can study the spatial distribution of the released drug, with a localization around the inserted site under the fluidic flow after 24 hours. We confirmed the spatially defined drug (rhodamine B) release in this microfluidic device using a fluorescent microscope and by imaging the distribution of fluorescent signals in the channel and in the macrophages.

Cell biocompatibility assay for the 3D-BPH nanoscaffolds: To examine the biocompatibility of 3D-BPH nanoscaffolds, a Transwell®-based system was used. Briefly, iPSC-NSCs were cultured in growth media on the bottom layer with laminin coating and the 3D-BPH nanoscaffold was incubated on the top layer of the membrane. Cells adhered and proliferated for 2 days before the top layer was removed and the cytotoxicity assay was performed. In our experiments, Presto Blue-based cytotoxicity assay was used and the ultraviolet-visible (UV-Vis) absorption at 570 nm was applied for quantifying cell viabilities.

Effects of anti-inflammatory drugs on neural cells*:* One advantage of 3D-BPH nanoscaffolds is their ability to combine 3D biomimicry ECM with the delivery of anti-inflammation drugs to enhance neurogenesis. As most corticoid drugs present side effects at high dosages, it is essential to deliver the proper amount of MP for *in situ* enhancement of neurogenesis of iPSC-NSCs inside the scaffold. To this end, we studied the dosage-dependent effects of MP on the proliferation and differentiation of iPSC-NSCs. We seeded and cultured iPSC-NSCs (40,000 cells per well) on laminin-coated 48 well plates in growth media for one day, followed by media change into bFGF-added and bFGF-free media for proliferation and differentiation assays, respectively. Two days after, cells in the proliferation assay were treated with PrestoBlue reagents with UV-Vis absorption at 570 nm recorded. Cell

viability from MP treatment at varying concentrations was quantified by normalizing to the control (growth media only). For the differentiation assay, mRNAs from cells were harvested 7 days after the bFGF withdrawal and analyzed by qRT-PCR. Relative levels of TuJ1 and GFAP were calculated and compared between the MP-treated cells and control cells.

HPLC Analysis: To study the release of methylprednisolone from the scaffold, 20μL of the solution, collected from the supernatant with MP released from the 3D-BPH, was directly injected into HPLC for quantification. The HPLC analysis was performed by using an Agilent 1260 infinity series HPLC with a diode array detector (DAD) (Santa Clara, CA, USA). The separation was carried out on a Phenomenex Luna® 5 μm C18 Column (75 x 4.6 mm, 5μm) (Torrance, CA, USA) using a gradient elution method. The mobile phase composed of aqueous solution of 0.1% (v/v) formic acid (Solvent A) and 0.1% (v/v) formic acid in acetonitrile (Solvent B). The elution condition was 95% A decreased to 70% in 2 minutes, then decreased to 20% A in 6 minutes, and maintained for 1 minute at a constant flow rate of 1 mL/min. The signals were detected at 240nm, 250nm, and 254 nm. The methylprednisolone peak was identified using the standard solutions prepared in phosphate buffer (PBS). The quantification of MP was calculated based on a calibration curve constructed from a series of standard solutions.

Gene Expression Analysis: Total RNA was extracted using TRIzol Reagent (Life Technologies) and transcribed to cDNA for quantitative PCR (qPCR) analysis. Specifically, cDNA was generated from 1 μg of total RNA using the Superscript III First-Strand Synthesis System (Life Technologies). The qPCR reactions were performed using Power SYBR Green PCR Master Mix (Applied Biosystems) on a StepOnePlus Real-Time PCR System (Applied Biosystems) with the primers specific to each of the target mRNAs. The resulting Ct values were normalized to GAPDH. Standard cycling conditions were used for all reactions with a melting temperature of 60°C. All primers were obtained from the PrimerBank database [9-11] and listed in TABLE S1.

B. SUPPORTING FIGURES:

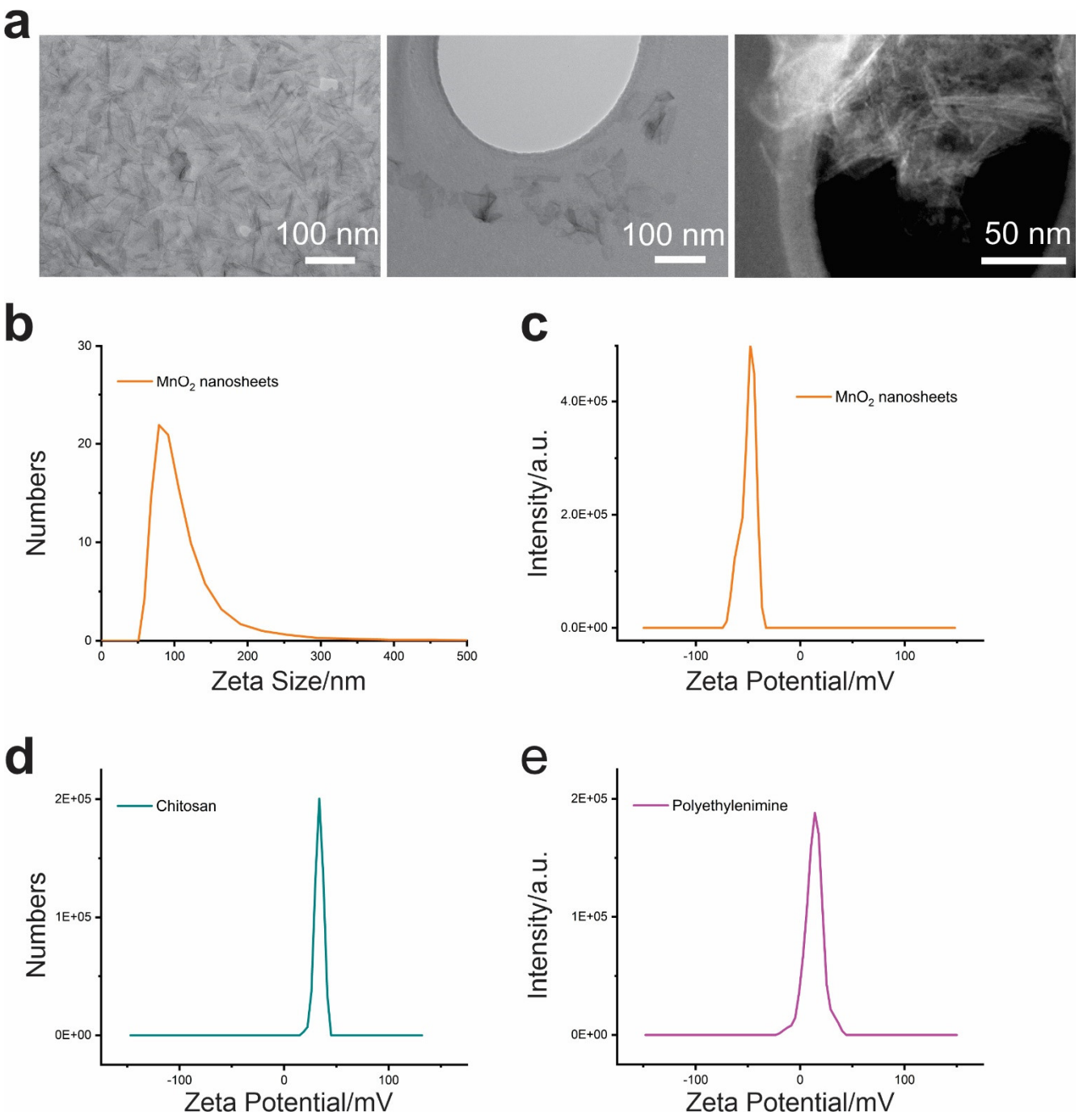

FIGURE S1. Characterization of anionic biodegradable nanomaterials (MnO_2 nanosheets) and cationic polymers for the LBL electrostatic 3D assembly-based synthesis of 3D-BPH nanoscaffolds. a, Transmission electron microscope (TEM) of MnO_2 nanosheets illustrating their atomic-thin structures. **b-c**, Hydrodynamic size (**b**) and negative Zeta potential (**c**) of the MnO_2 nanosheets. **d-e**, Cationic charges of chitosan and polyethyleneimine (PEI) confirmed by Zeta potential measurement. Y-axis indicates the signal intensity at assigned zeta potential values (X-axis).

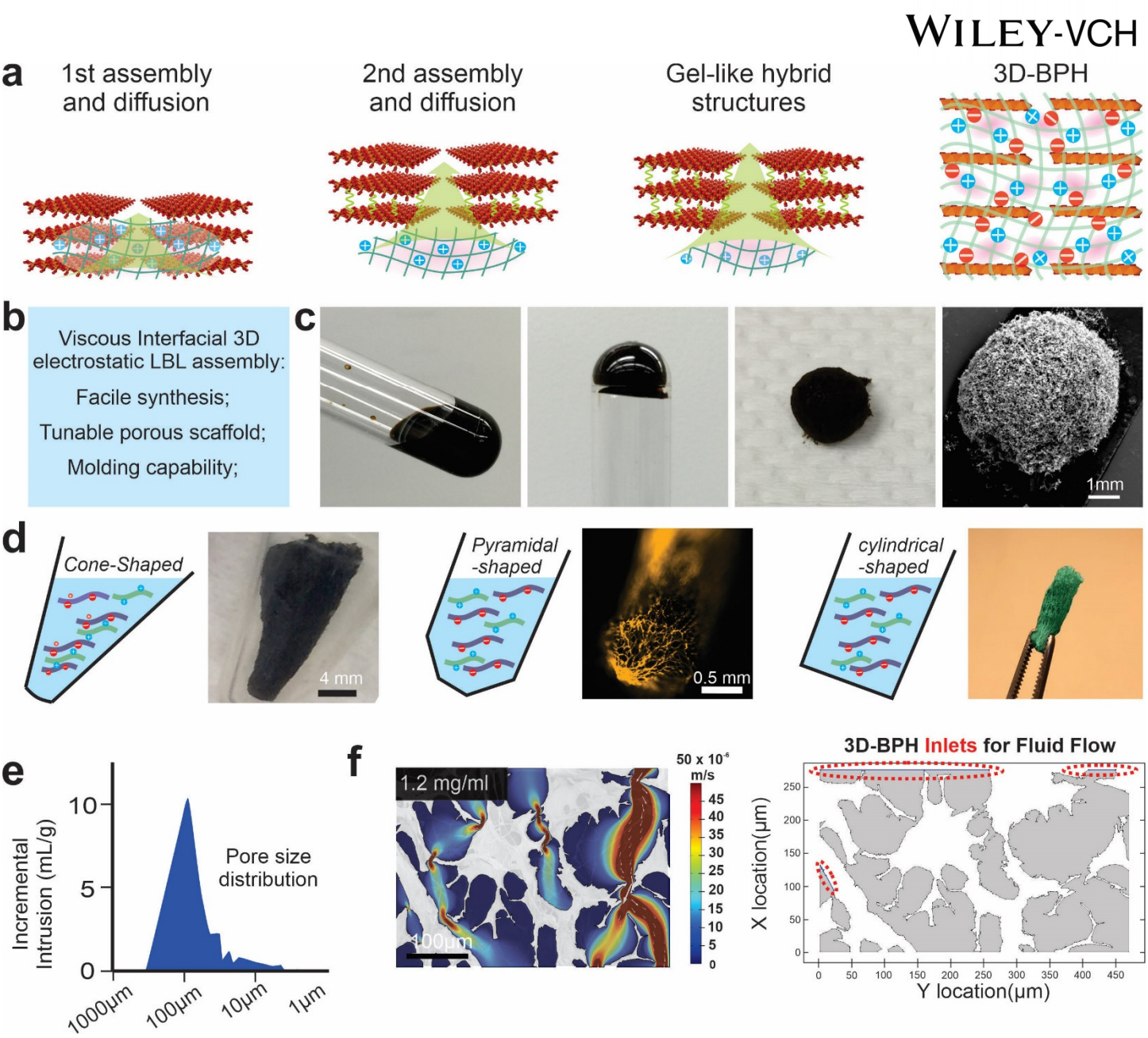

FIGURE S2. Synthesis and characterization of the 3D-BPH nanoscaffold. a, A schematic diagram illustrating the mechanism of viscous interfacial electrostatic 3D assembly for synthesizing the 3D-BPH nanoscaffold. **b**, Advantages of viscous interfacial electrostatic 3D assembly for synthesizing the 3D-BPH nanoscaffold. **c**, The assembly process of the viscous interfacial electrostatic 3D assembly based on photographs (left 3 images) and SEM. **d**, Molding capability of the viscous interfacial electrostatic 3D assembly for synthesizing shape-defined 3D-BPH nanoscaffolds. **e**, Mercury porosimetry measurement of the 3D-BPH nanoscaffolds. **f**, COMSOL® simulation on the porous structure of the 3D-BPH nanoscaffold. Scale bar: 100 μm. The scaffold condition is fabricated from the condition with 2D-MnO_2 nanosheets at a concentration of 1.2 mg/mL.

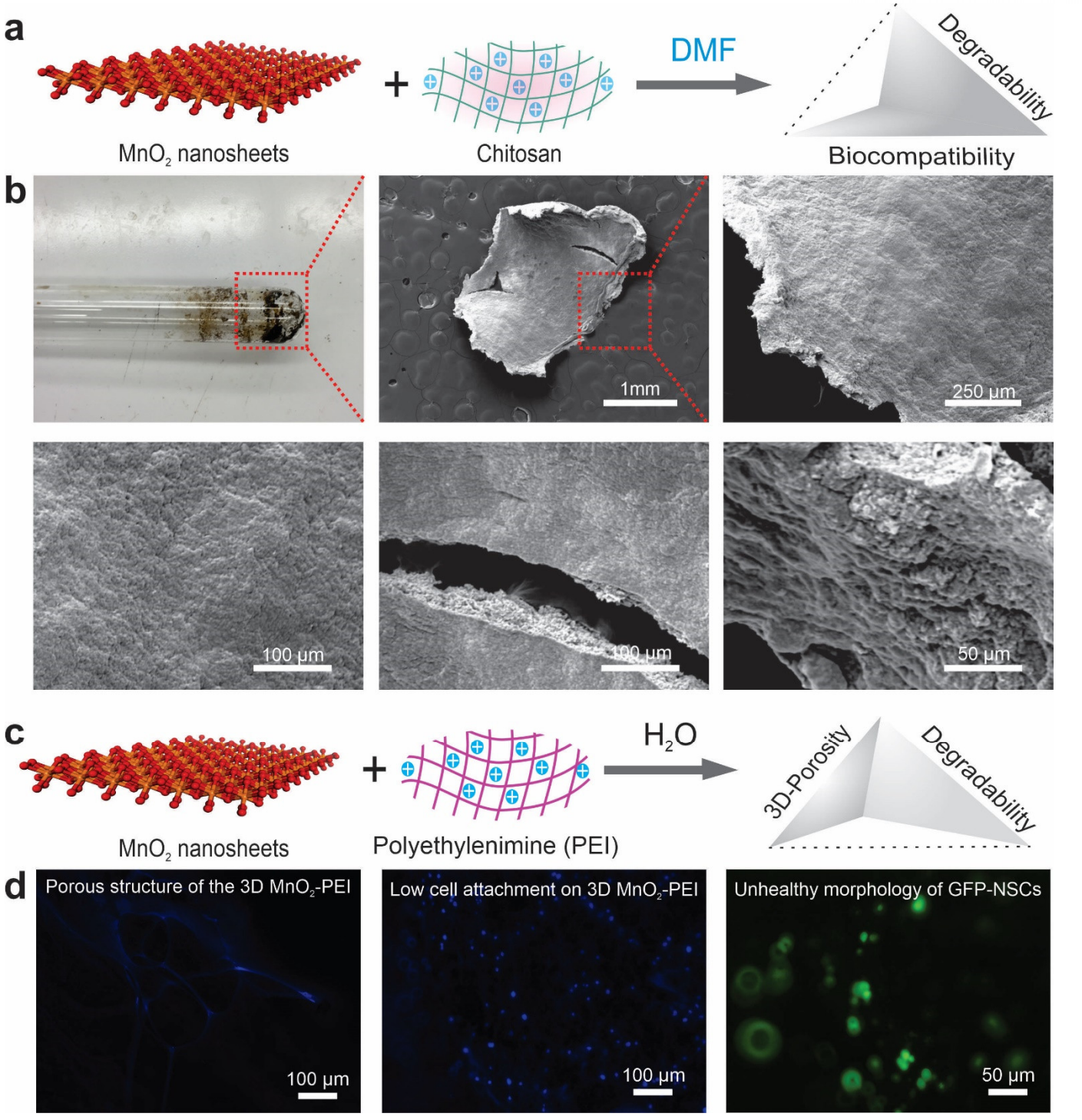

FIGURE S3. Generalized synthesis of nanomaterial assemblies using LBL electrostatic 3D assembly. a-b, A schematic diagram (**a**), photograph (top left image of **b**) and scanning electron microscope (SEM, **b**) images of a non-porous scaffold synthesized by LBL electrostatic 3D assembly when DMF is used as a solvent instead of water. **c-d**, A schematic diagram (**c**) and unhealthy cell morphologies of NSCs cultured on non-porous 3D-BPH nanoscaffolds synthesized using PEI instead of chitosan.

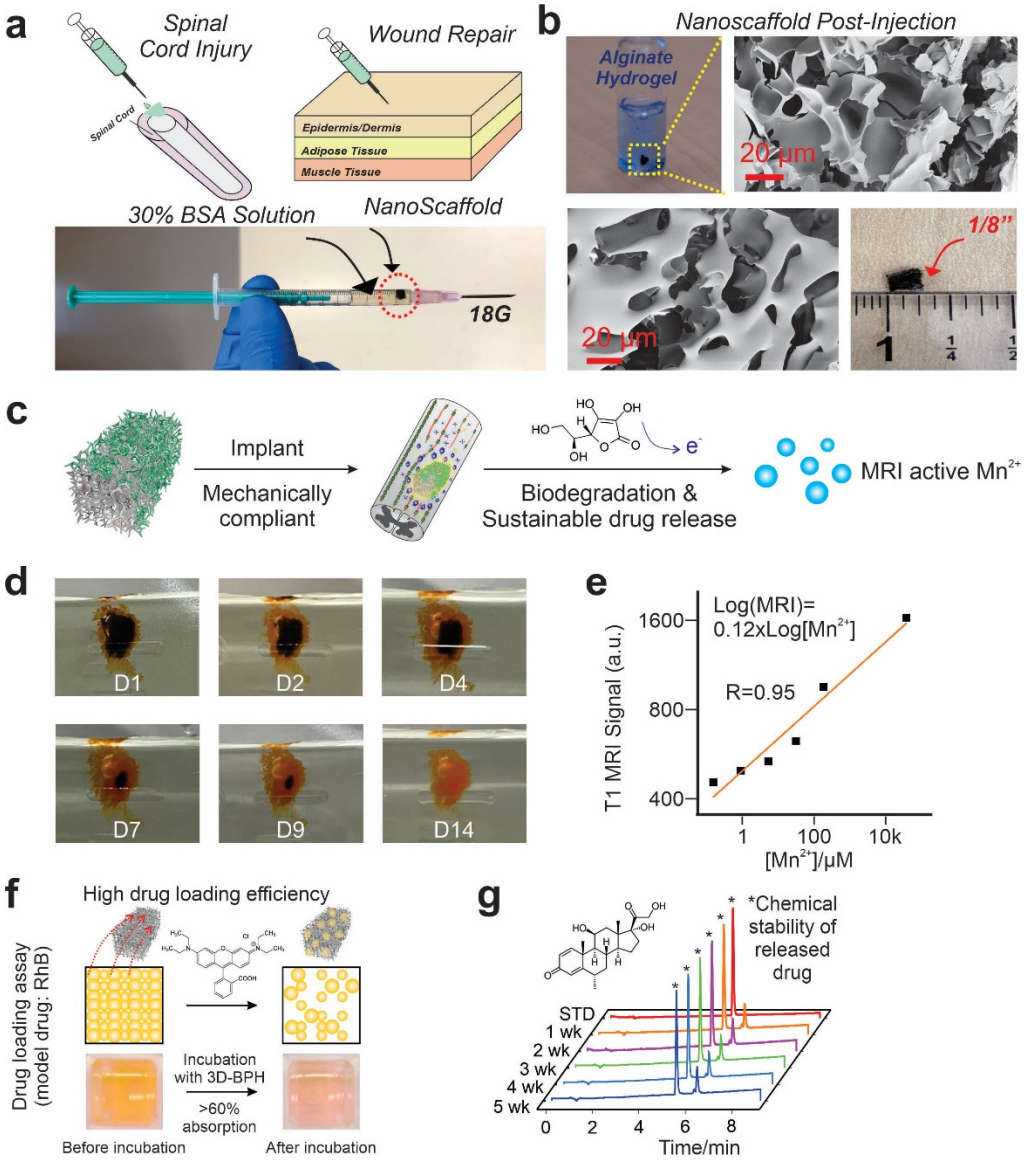

FIGURE S4. Injectable 3D-BPH nanoscaffold with the capability of releasing MRI contrasting agents and maintaining the chemical stability of drugs during degradation and drug releasing. a, A schematic diagram (image on top) and photograph (image in the bottom) illustrating the injectable 3D-BPH nanoscaffold and the loading into an 18-gauge syringe. Please note we only tested a scaffold with a relatively simple shape here and it remains to be examined whether a personalized spinal cord shape with higher complexity can be well maintained after flowing through the syringe due to the shear forces. **b**, SEM image showing the preserved 3D porous structure of the 3D-BPH nanoscaffold after injecting through an 18-gauge syringe. **c**, Schematic diagram illustrating the degradation of 3D-BPH nanoscaffold and the release of MRI active Mn^{2+}. **d**, Photographs showing the time-dependent degradation of 3D-BPH at physiologically relevant redox conditions (10 μg/mL ascorbic acid). **e**, A Calibration curve of Mn ion concentration-dependent T1 MRI signal. **f**, High drug loading efficiency of the 3D-BPH nanoscaffolds confirmed by the differences of fluorescence intensity of Rhodamine B before and after absorption onto scaffolds. **g**, The stability of a clinically used neuroprotective drug, Methylprednisolone (MP), released from 3D-BPH was maintained compared to the standard (STD), characterized by UV-Vis absorption spectroscopy.

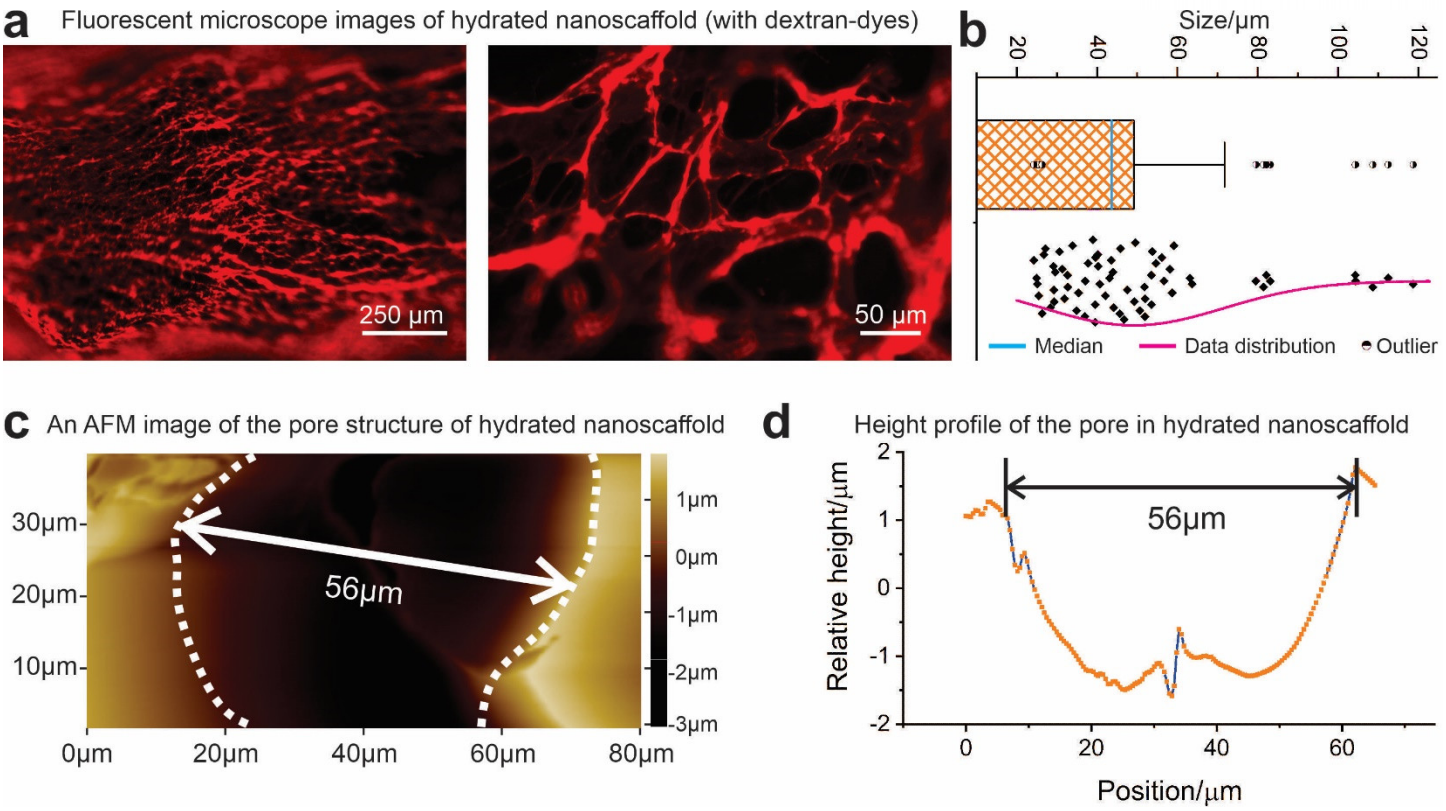

FIGURE S5. Characterization of porous structure of 3D-BPH nanoscaffold under hydrated conditions. **a**, Zoomed out (left) and zoomed in (right) fluorescence images of 3D-BPH nanoscaffold synthesized from the condition with 2.4 mg/mL MnO_2 nanosheet concentration (corresponding to the pore size condition of 50 μm). **b**, Summarized result on the pore size distribution automatically analyzed by the Nikon NIS Element software. These results show an average pore size slightly below 50 μm (47 μm) and are similar with the lyophilized scaffold. **c**, The characterization of a representative pore of 3D-BPH nanoscaffold (synthesized from the condition with 2.4 mg/mL MnO_2 nanosheet concentration) under hydrate conditions (incubated with PBS) by AFM using a liquid cell set-up. **d**, A height profile of the AFM imaging on the hydrated 3D-BPH nanoscaffold in **c**. The depth of each pore is 2-3 μm, with pore size around 50 μm that is consistent with what we observed in the FE-SEM.

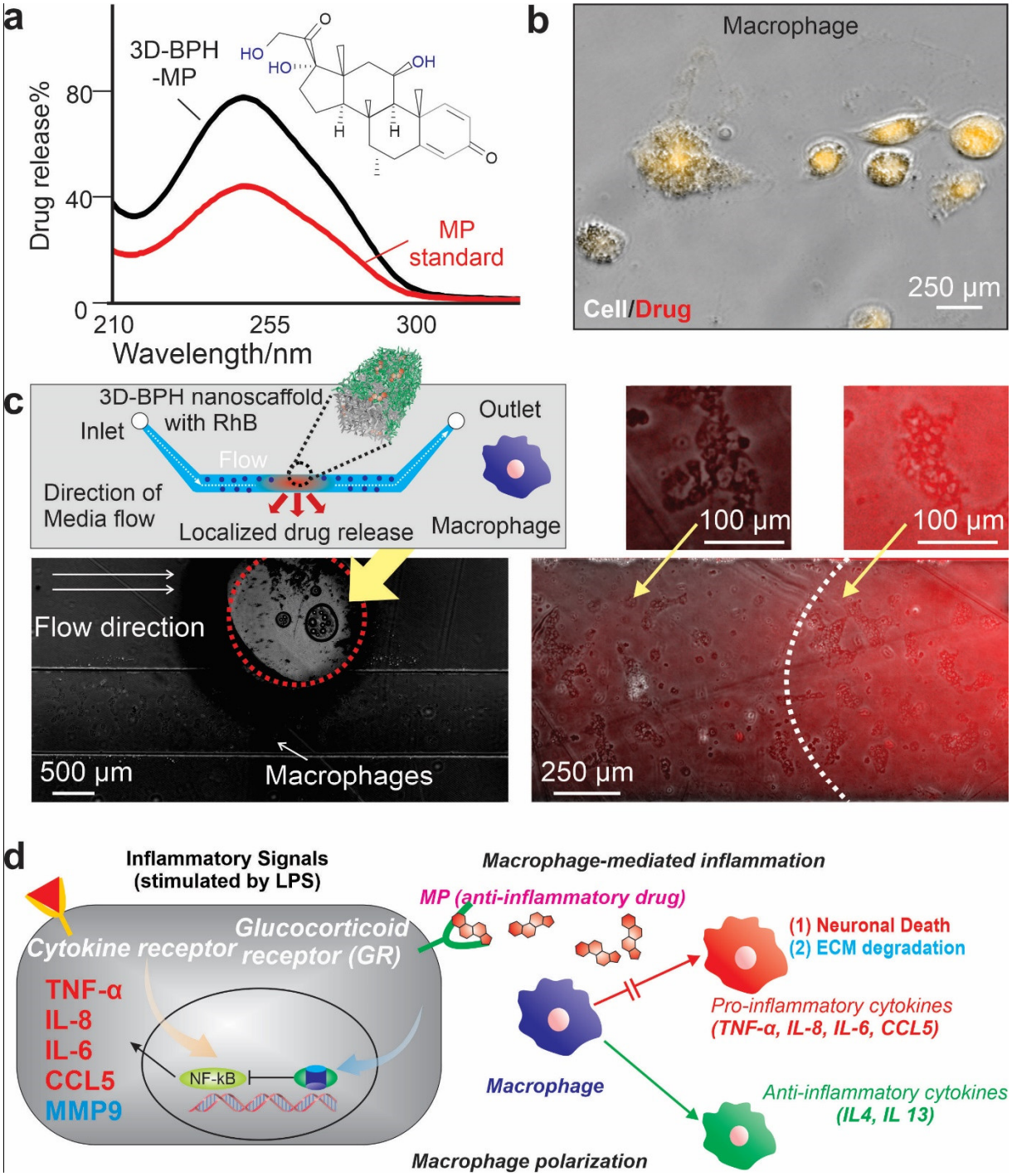

FIGURE S6. Drug stability and the spatially controlled release of drugs by 3D-BPH nanoscaffold. a, UV-Vis spectrum showing the good stability of MP drug released from the nanoscaffold based on the consistent absorption peaks before and after the loading and release. **b**, Fluorescent and optical microscope images of macrophages uptaking a **model** drug (rhodamine B, RhB). **c**, A microfluidic-based device for monitoring the spatially controlled drug release under the media flow. **d**, Mechanistic insight into MP-based gene regulation on guiding the pro-inflammatory macrophages [stimulated by lipopolysaccharide (LPS)] polarized toward anti-inflammatory macrophages. Pro-inflammatory macrophages secret inflammatory cytokines and ECM-degrading enzymes (MMP) that may reduce neural survival rate and axonal growth after CNS injuries.

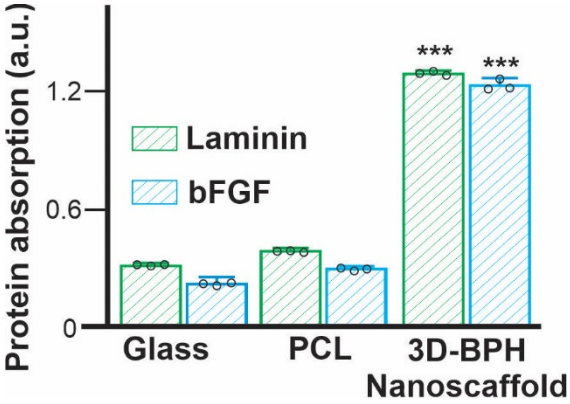

FIGURE S7. Enhanced protein (laminin and bFGF) absorption by 3D-BPH nanoscaffold (synthesized from the 2.4 mg/mL MnO_2 concentration), as characterized by BCA protein binding assay, by subtracting the amount of protein before and after incubation of the scaffolds. The incubation time is 24 hours. Error bars represent standard around the mean. n=3 experimental replicates. ***P<0.001 by one-way ANOVA with Tukey post-hoc analysis.

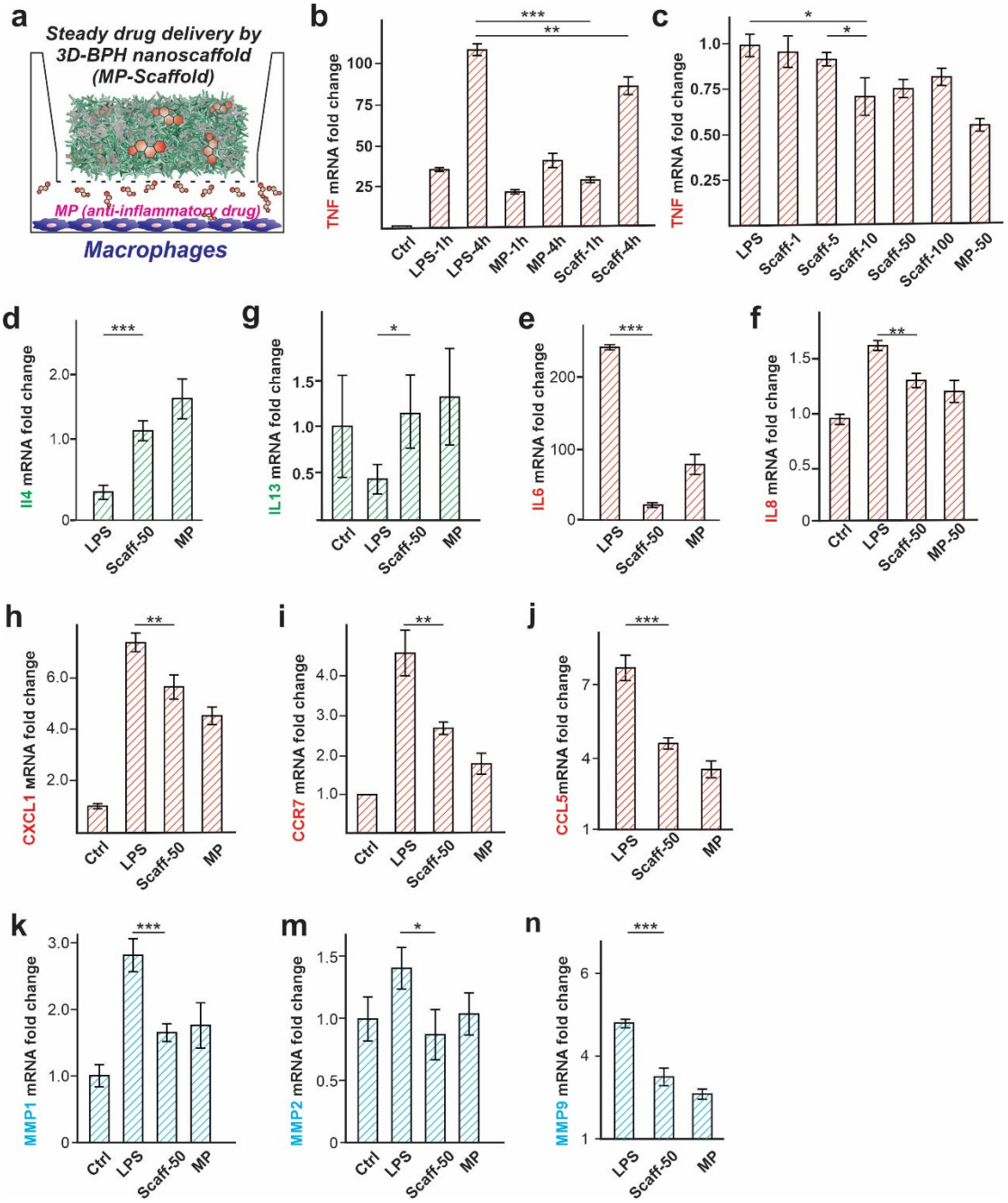

FIGURE S8. Anti-inflammatory effects from MP-loaded 3D-BPH nanoscaffold based on qRT-PCR measurements. Error bars are standard deviation around the mean. n=3 biological replicates. *P<0.05, **P<0.01, ***P<0.001 by one-way ANOVA with Tukey post-hoc analysis. Ctrl means control experiment of macrophage culture without treatment of LPS. Scaff-1, Scaff-5, Scaff-10, Scaff-50, Scaff-100, refer to the conditions of LPS-stimulated macrophages treated by varying 3D-BPH nanoscaffold (pore size of 50 μm synthesized from MnO_2 concentration of 2.4 mg/mL) loaded with drug (MP) concentration conditions at 1 μg/mL, 5 μg/mL, 10 μg/mL, 50 μg/mL, and 100 μg/mL, respectively. MP-50, as a positive control, refers to the condition that macrophages were directly treated with a media containing free MP drugs at a concentration of 50 μg/mL. In **c**, **d**, **e**, **j**, **n**, the LPS, Scaff-50, MP results are all normalized to the control condition (macrophage without LPS treatment).

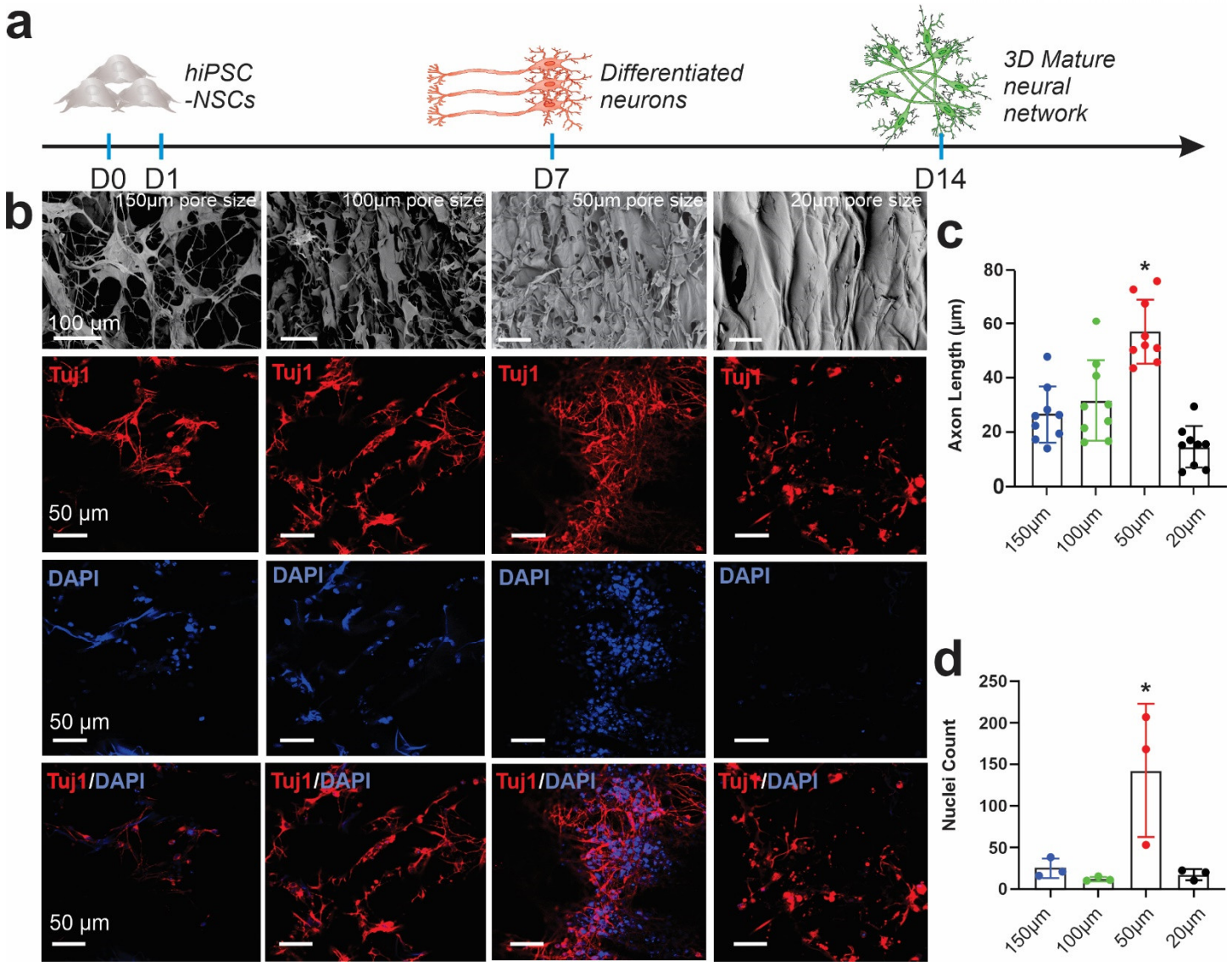

FIGURE S9. Porous structures-dependent neuronal differentiation on 3D-BPH nanoscaffolds. a, A schematic diagram showing the timeline of the neuronal differentiation process of the iPSC-NSCs seeded on the 3D-BPH nanoscaffold. **b-d**, Immunostaining images showing the structure-dependent neuronal differentiation (differentiated for 7 days) (**b**) and quantifications on axonal length (**c**) and nuclei counts (**d**) on 3D-BPH nanoscaffolds. n=9 and 3 technical replicates for graphs shown in **c** and **d**, respectively. Error bars represent standard deviation around the mean. P*<0.05, by one-way ANOVA. In panel **b**, the labelling of 150 μm, 100 μm, 50 μm, and 20 μm refer to the pore size of 3D-BPH nanoscaffolds synthesized from 2D-MnO_2 nanosheet concentrations at 1.2 mg/mL, 1.8 mg/mL, 2.4 mg/mL, and 3.0 mg/mL, respectively which is consistent with FIGURE 3. By performing this study, we confirmed the highest axonal elongation on the 50 μm pore size (synthesized from the condition of 2.4 mg/mL 2D-MnO_2 nanosheets) 3D-BPH nanoscaffold condition.

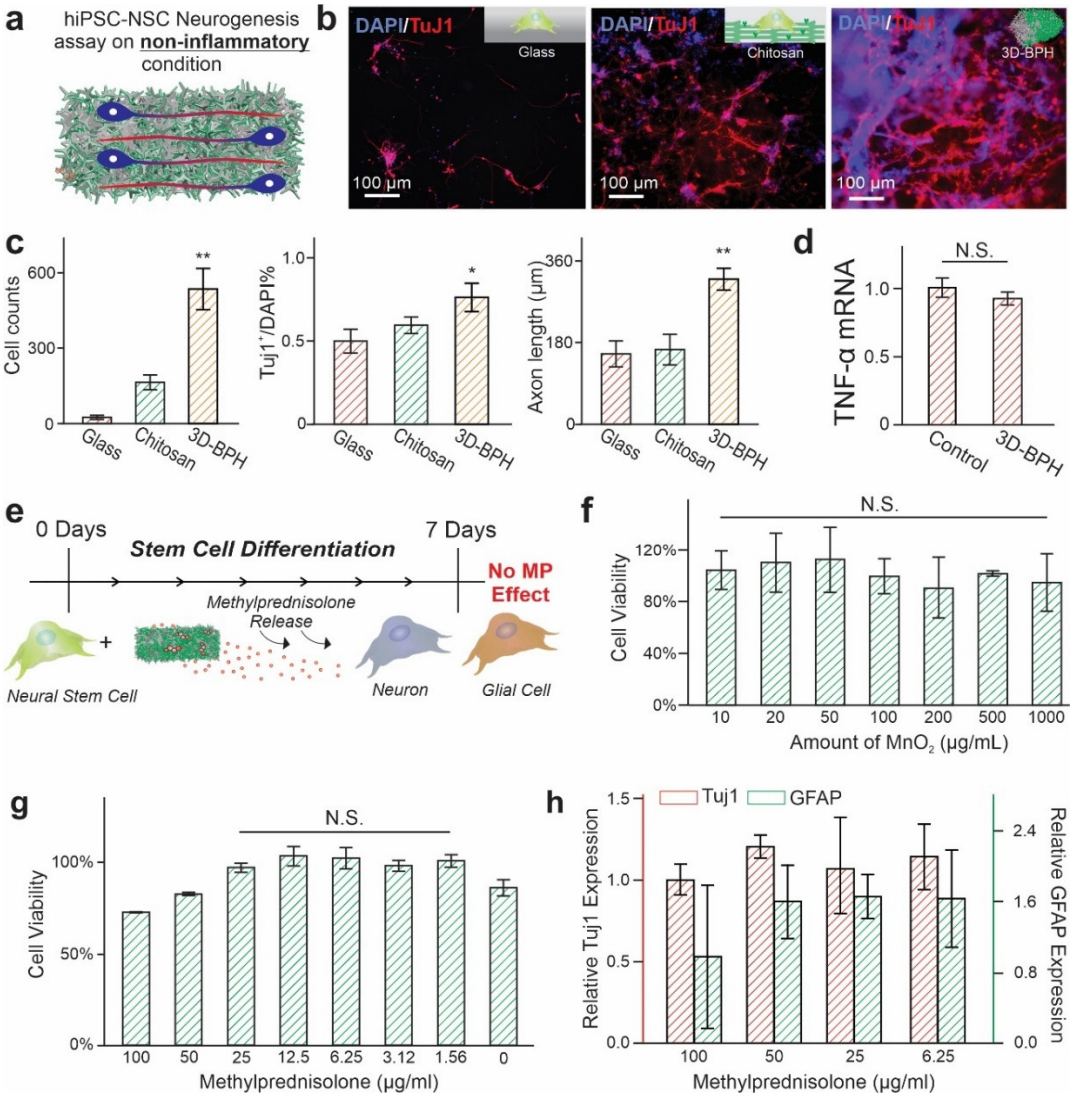

FIGURE S10. Enhanced neuronal differentiation on 3D-BPH nanoscaffolds and the biocompatibility of 3D-BPH nanoscaffold and methylprednisolone (MP). **a**, A schematic diagram illustrating the stem cell neuronal differentiation assay under healthy culture (non-inflammatory) conditions. **b-c**, Representative immunostaining images (**b**) and quantifications (**c**) on cell numbers, percentages of neurons and axon lengths of neurons differentiated from hiPSC-NSCs cultured on 3D-BPH nanoscaffolds as compared to control scaffolds. 3D-BPH means 3D-BPH nanoscaffold. **d**, The effect of 3D-BPH nanoscaffold (synthesized from 2.4 mg/mL MnO_2 nanosheet condition with an average pore size of 50 μm) on the inflammatory gene (TNF) expression in macrophages. The values are normalized to the control (no treatment). **e**, Timeline of the toxicity assay and differentiation assay to study the biocompatibility of 3D-BPH nanoscaffold and MP. **f**, Summarized results for the biocompatibility assay on the concentration-dependent 3D-BPH nanoscaffolds quantified by the amount of MnO_2 using a Presto Blue®-based cell viability assay. **g**, Relative cell viabilities under varying concentrations of methylprednisolone to confirm its minimal toxicity on iPSC-NSCs (normalized to the no treatment control condition). **h**, qRT-PCR experiment results showing the minimal difference of stem cell differentiation when treated by methylprednisolone at different concentrations regarding its effect on neuronal differentiation of iPSC-NSCs. Error bars are standard deviation around the mean. n=3 experimental replicates for **c-h**. *P<0.05, **P<0.01, N.S. means no significance by student's t test (**d**) or one-way ANOVA (**c**, **f**, **g**) with Tukey post-hoc analysis.

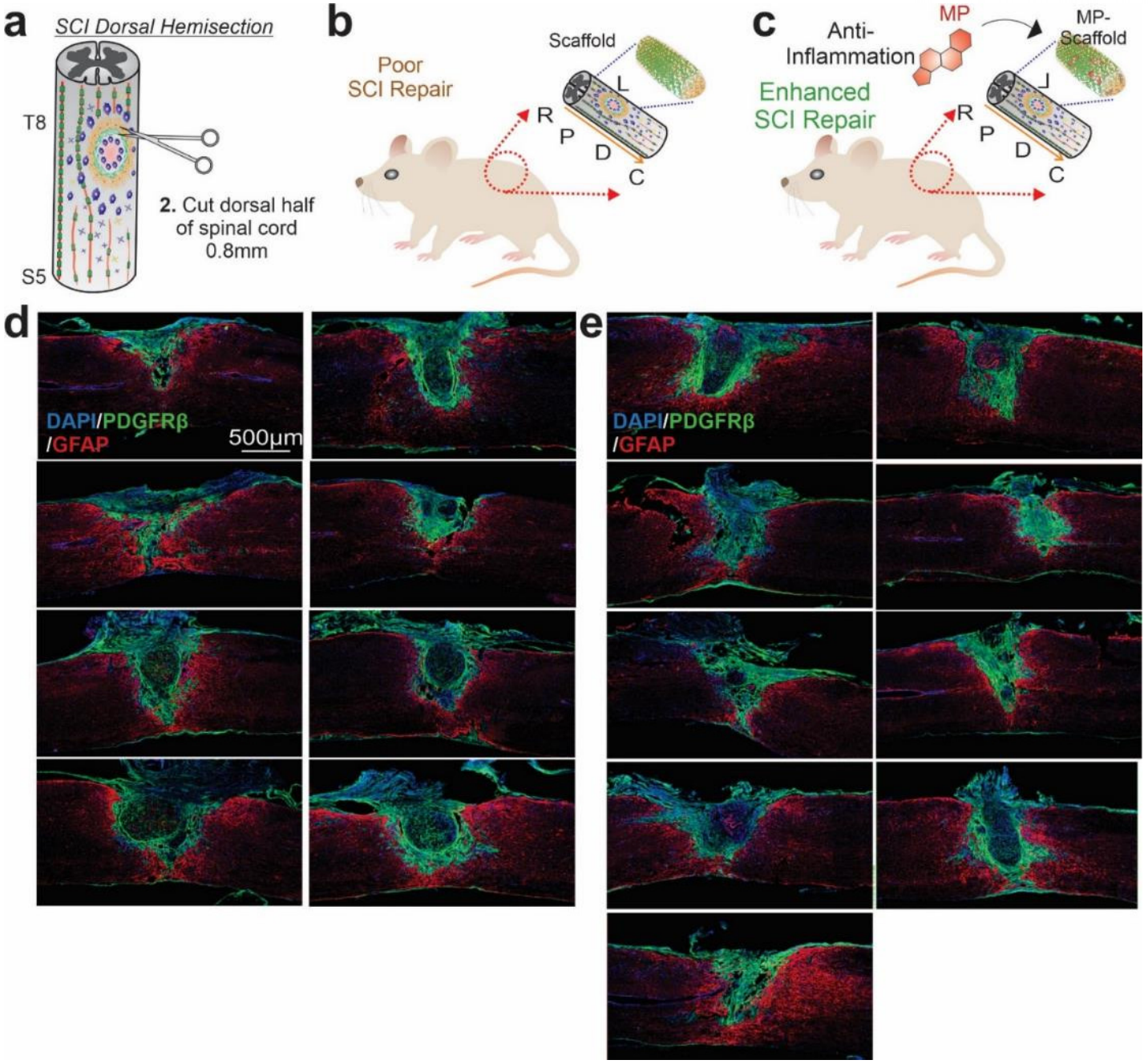

FIGURE S11. Astroglial and fibrotic scar formation after injuries followed by the implantation of 3D-BPH and MP-loaded 3D-BPH nanoscaffold. a, Schematic diagram showing the surgical procedure for the creation of hemisection SCI models. **b-e**, Schematic diagrams (**b-c**) and immunostaining images (**d-e**) of 3D-BPH nanoscaffold (**b, d**) and MP-3D-BPH nanoscaffold implanted SCI sites (**c, e**).

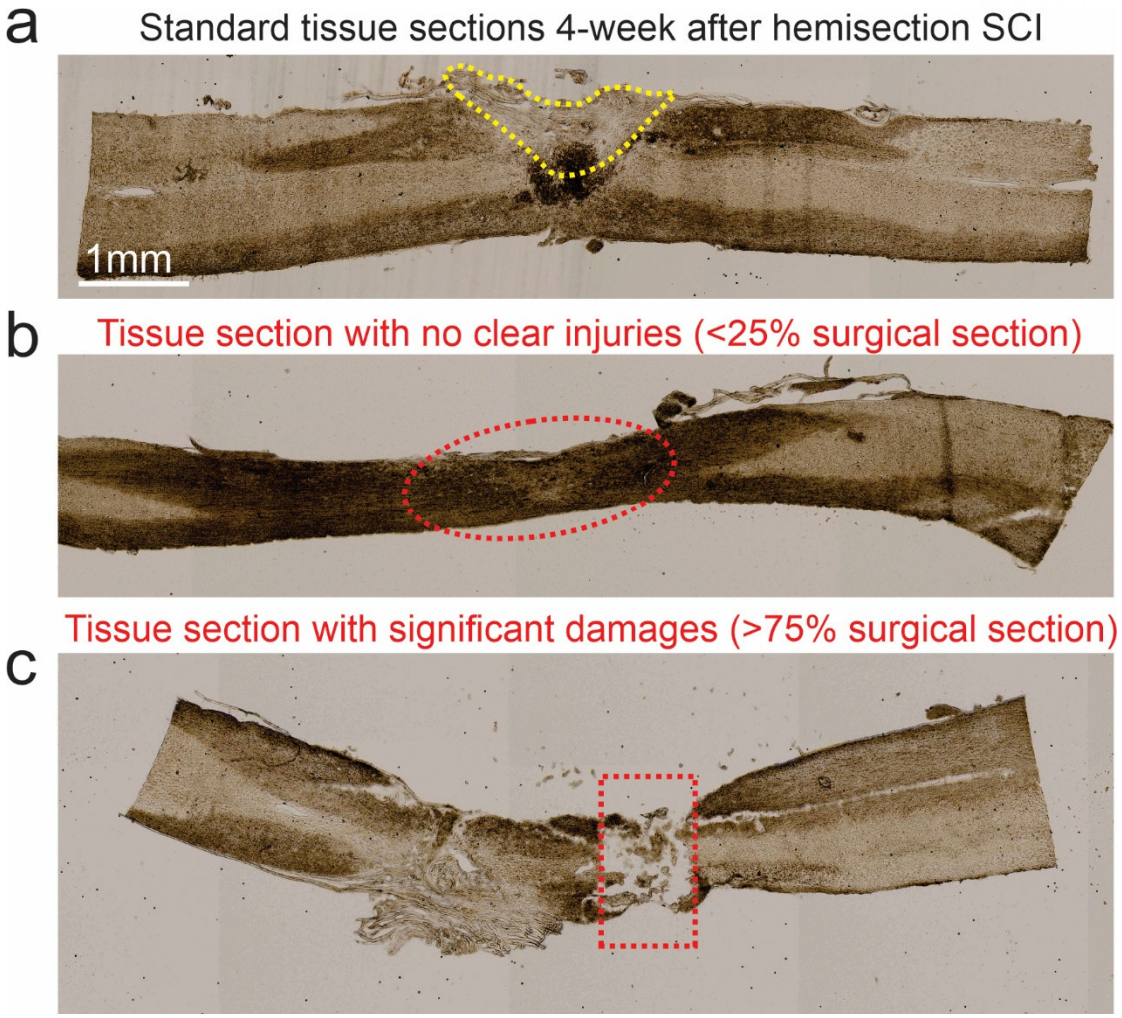

FIGURE S12. Screening criteria for the *in vivo* immunostaining analysis based on the tissue slice qualities. **b** and **c** have the same scale bar as in **a**.

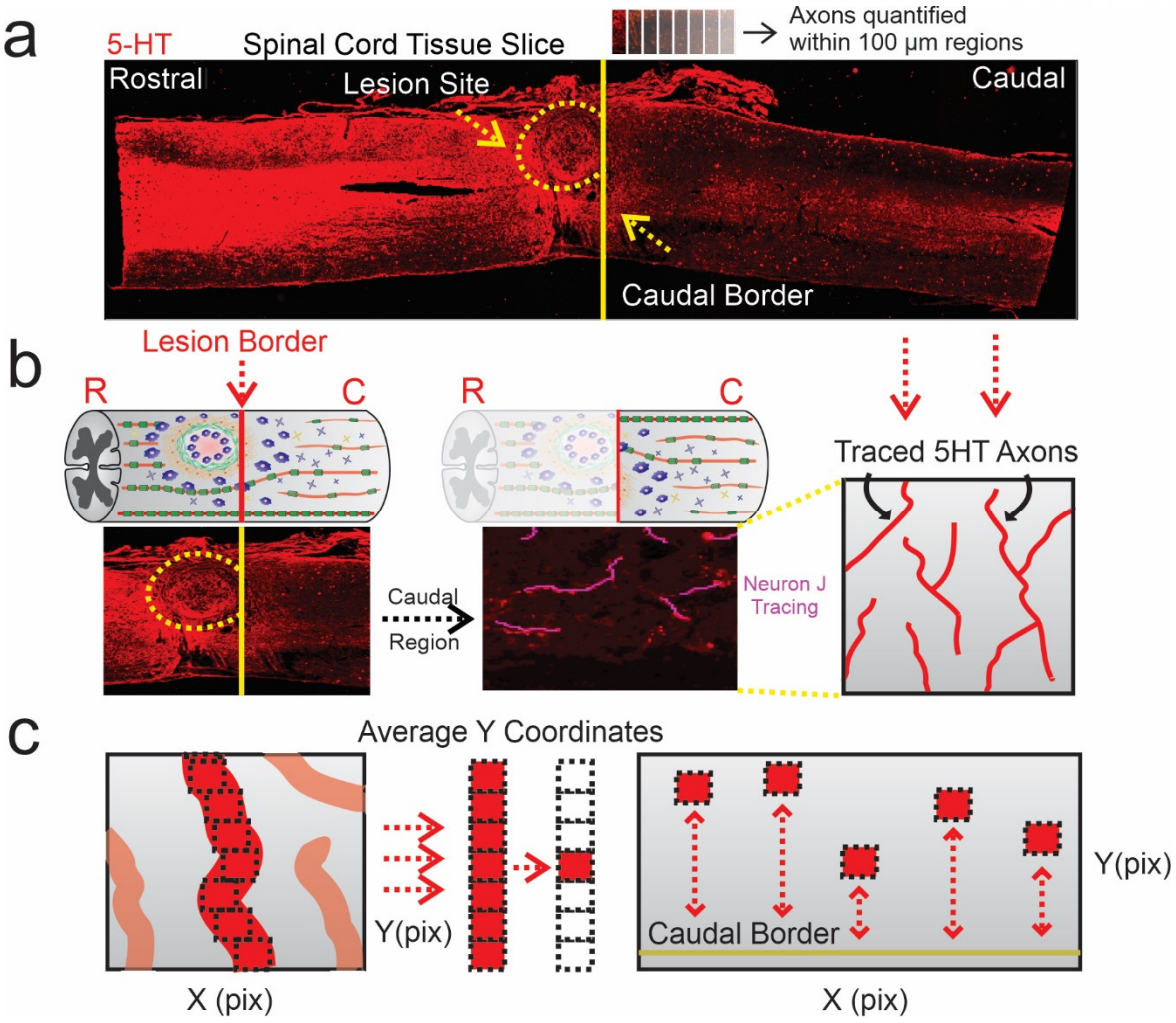

FIGURE S13. The methodology of 5-HT axon quantification in spinal cord tissue slices four weeks after 3D-BPH and MP-loaded 3D BPH nanoscaffold transplantation. a, Spinal cord tissue slice exhibiting 5-HT (red) staining while depicting lesion site boundary and caudal border. Average axon number within 100 µm regions beginning at the border was quantified over 4-5 2D sagittal tissue sections for each animal and depicted in FIGURE 6e. **b**, Schematic diagrams showing the semi-automated tracing of 5-HT axons. **c**, Schematic diagram showing the pixelization of an individual axon and averaging of Y coordinates to determine a midpoint within the caudal region of the spinal cord.

C. SUPPORTING TABLES:

Species	Targets	Forward Primer (5' to 3')	Reverse Primer (5' to 3')
human	GAPDH	CCGCATCTTCTTTTGCGTCG	GCCCAATACGACCAAATCCGT
human	CCL5	CCCCATATTCCTCGGACACC	AGCACTTGCCACTGGTGTAG
human	CCR7	TGAGGTCACGGACGATTACAT	GTAGGCCCACGAAACAAATGAT
human	CXCL1	TCACAGTGTGTGGTCAACAT	AGCCCCTTTGTTCTAAGCCA
human	GFAP	AGGAAGATTGAGTCGCTGGA	AACCTCCTCCTCGTGGATCT
human	IL4	CCAACTGCTTCCCCCTCTG	TCTGTTACGGTCAACTCGGTG
human	IL6	AAACAACCTGAACCTTCCAAAGA	GCAAGTCTCCTCATTGAATCCA
human	IL8	ACTGAGAGTGATTGAGAGTGGAC	AACCCTCTGCACCCAGTTTTC
human	IL13	GAGGATGCTGAGCGGATTCTG	CACCTCGATTTTGGTGTCTCG
human	MMP1	AAAATTACACGCCAGATTTGCC	GGTGTGACATTACTCCAGAGTTG
human	MMP2	TACAGGATCATTGGCTACACACC	GGTCACATCGCTCCAGACT
human	MMP9	TGTACCGCTATGGTTACACTCG	GGCAGGGACAGTTGCTTCT
human	TNF	CTGCTGCACTTTGGAGTGAT	AGATGATCTGACTGCCTGGG
human	TUBB3	GGCCAAGGGTCACTACACG	GCAGTCGCAGTTTTCACACTC
mouse	TNF	AGGCACTCCCCCAAAAGATG	TCACCCCGAAGTTCAGTAGAC
mouse	IL-1b	CTTCAAATCTCACAGCAGCAGCACATC	CCACGGGAAAGACACAGGTAG
mouse	IL-6	AACCACGGCCTTCCCTACTTCA	TCATTTCCACGATTTCCCAGAG
mouse	CCL5	TGCCCACGTCAAGGAGTATTTCTA	TGGCGGTTCCTTCGAGTGACAA
mouse	GAPDH	TGGCCTTCCGTGTTCCTAC	GAGTTGCTGTTGAAGTCG

TABLE S1: Table of the primers used for quantitative PCR for *in vitro* cell studies (human species) and *in vivo* animal studies (mouse species). All primers were obtained from the PrimerBank database[1-3].

CNS	Central Nervous System	**ECM**	Extracellular Matrix	**3D**	Three Dimensional
hiPSC	Human Induced Pluripotent Stem Cell	**SCI**	Spinal Cord Injury	**BPH**	Biodegradable Porous Hybrid
MRI	Magnetic Resonance Imaging	**NSC**	Neural Stem Cell	**LBL**	Layer-by-Layer
MnO2	Manganese Dioxide	**FDA**	Food and Drug Association	**Mw**	Molecular Weight
GO	Graphene oxide	**PEI**	Polyethyleneimine	**FE-SEM**	Field Emission Scanning Electron Microscope
LPS	Lipopolysaccharide	**MP**	Methylprednisolone	**RhB**	Rhodamine B
FGF	Fibroblast Growth Factor	**T8**	Thoracic 8	**TNF**	Tumor Necrosis Factor
IL	Interleukin	**CCL**	Chemokine Ligands	**MMP**	Metalloproteinase
SYN	Synapsin	**CD11b**	Cluster of Differentiation Molecule 11b	**PDGFR β+**	Platelet-Derived Growth Factor Subunit β
TuJ1	Human β-Tubulin 3	**MAP2**	Microtubule-associated protein 2	**NeuN**	Hexaribonucleotide Binding Protein-3
GFAP	Glial Fibrillary Acidic Protein	**5-HT**	5-Hydroxytryptamine	**BMS**	Basso Mouse Scale
wt%	Weight percentage	**rpm**	Revolutoin Per Minute	**TMAOH**	Tetramethylammonium hydroxide pentahydrate
TEM	Transmission Electron Microscopy	**PBS**	Phosphate Buffered Saline	**DMSO**	Dimethyl Sulfoxide
AFM	Atomic Force Microscope	**BCA**	Bicinchoninic Acid Assay	**PCL**	Polycaprolactone
PMA	Phorbol 12-Myristate 13-Acetate	**qRT-PCR**	Quantitative Real Time-Polymerase Chain Reaction	**i.p.**	Intraperitoneal
DPEC	Diethylpyrocarbonate	**UV-Vis**	Ultraviolet-visible	**DMF**	Dimethyl Formamide
FBS	Fetal Bovine Serum	**CT**	Cycle Threshold	**PFA**	Paraformaldehyde

TABLE S2. Full names of abbreviated terminologies.

D. REFERENCES CITED IN THE SUPPORTING INFORMATION:

[1] L. Rey, Freeze-drying/lyophilization of pharmaceutical and biological products, *CRC Press*, **2016**.

[2] N. Massad‐Ivanir, G. Shtenberg, T. Zeidman, E. Segal, *Advanced Functional Materials* **2010**, 20, 2269.

[3] G. L. Ying, N. Jiang, S. Maharjan, Y. X. Yin, R. R. Chai, X. Cao, J. Z. Yang, A. K. Miri, S. Hassan, Y. S. Zhang, *Advanced Materials* **2018**, 30, 1805460.

[4] C. S. Verbeke, D. J. Mooney, *Advanced healthcare materials* **2015**, 4, 2677.

[5] Q. Zhang, J. Kang, Z. Xie, X. Diao, Z. Liu, J. Zhai, *Advanced Materials* **2018**, 30, 1703323.

[6] A. J. Salgado, J. M. Oliveira, A. Martins, F. G. Teixeira, N. A. Silva, N. M. Neves, N. Sousa, R. L. Reis, in Tissue Engineering of the Peripheral Nerve: Stem Cells and Regeneration Promoting Factors, Vol. 108 (Eds: S. Geuna, I. Perroteau, P. Tos, B. Battiston), *Elsevier Academic Press Inc*, San Diego **2013**, 1.

[7] S. Shah, P. T. Yin, T. M. Uehara, S. T. D. Chueng, L. Yang, K. B. Lee, *Advanced Materials* **2014**, 26, 3673.

[8] A. F. Hagel, H. Albrecht, W. Dauth, W. Hagel, F. Vitali, I. Ganzleben, H. W. Schultis, P. C. Konturek, J. Stein, M. F. Neurath, *Journal of International Medical Research* **2018**, 46, 168.

[9] Wang, X., A PCR primer bank for quantitative gene expression analysis. *Nucleic acids research* **2003,** *31* (24), 154e-154.

[10] Spandidos, A.; Wang, X.; Wang, H.; Dragnev, S.; Thurber, T.; Seed, B., A comprehensive collection of experimentally validated primers for Polymerase Chain Reaction quantitation of murine transcript abundance. *BMC genomics* **2008,** *9*, 633.

[11] Spandidos, A.; Wang, X.; Wang, H.; Seed, B., PrimerBank: a resource of human and mouse PCR primer pairs for gene expression detection and quantification. *Nucleic acids research* **2010,** *38* (Database issue), D792-9.